JTTEE5 19:902–910
DOI: 10.1007/s11666-010-9504-1
1059-9630/$19.00 © ASM International

Peer Reviewed

Effect of Thermally Softened Bronze Matrix on the Fracturing Behavior of Diamond Particles in Hybrid Sprayed Bronze/Diamond Composite

Hyuntaek Na, Gyuyeol Bae, Kicheol Kang, Hyungjun Kim, Jay-Jung Kim, and Changhee Lee

(*Submitted September 9, 2009; in revised form March 17, 2010*)

In our previous study (Na et al., Compos Sci Technol 69:463-468, 2009), optimized thickness of protective nickel film was proposed for smaller diamond feedstock to obtain reduced impact stress and uniform flight behavior of particles during kinetic (or cold) spraying. However, in this study, nickel-coated diamond particles were severely fractured with increasing particle size due to high kinetic energy. Hence, an innovative hybrid spraying technique (a combination of kinetic and thermal spraying) was introduced to embed relatively large diamond particles into the bronze matrix. Size distributions of the diamond particles in the composite coatings were analyzed by scanning electron microscopy, an electron probe micro analyzer, and image analysis methods. In addition, impact behaviors of diamond particles in kinetic and hybrid gas flows were simulated through finite element analysis (ABAQUS/Explicit 6.7-2). Diamond fracturing was significantly minimized by the reduced impact energy afforded by the thermally softened bronze matrix through hybrid spraying.

Keywords diamond tool wheel, finite element analysis (FEA), hybrid spraying, kinetic (or cold) spraying, metal-matrix composites (MMCs)

1. Introduction

Diamond tools are typically used to abrade various tough materials such as ceramics, tungsten carbide, and stone because diamond possesses excellent mechanical properties including extremely high hardness, low frictional coefficient, and high wear resistance (Ref 1). Sintering has been commercially applied for manufacturing of diamond tool wheels. However, mechanical bonding between diamond and its metal binder decreases during sintering because diamond experiences oxidation at around 750 K in an oxygen atmosphere (Ref 2). Recently, a kinetic spraying technique for the manufacturing of diamond tool wheels has been introduced (Ref 3-5) that uses high-strain-rate impact with extremely low heat input during coating (Ref 6, 7). Therefore, it is a desirable method for depositing oxygen-sensitive materials such as diamond. Shin et al. (Ref 3) studied the deposition behavior of bronze/diamond composite feedstock with different kinetic spraying process parameters. VanSteenkiste et al. (Ref 4) investigated the fracture surfaces of kinetic sprayed aluminum/diamond composite coatings to determine the bonding between diamond particles and aluminum matrix. One of the most notable disadvantages of kinetic spraying is the difficulty in retaining the original diamond particle size distribution in the coating, as high velocity impacts during the process can cause fracturing of the diamonds. For this reason, application of a protective nickel film onto the diamond particles for uniform flight behavior and reduced impact stress was attempted in a previous study (Ref 5). However, the broken ratio of nickel-coated diamond particles increased sharply with increasing particle size due to high kinetic energy. To this end, an innovative hybrid spraying technique was used in this study to obtain novel bronze/diamond composite coatings with relatively large diamond particles (mean size: 80 μm without nickel film) by a reduced impact stress of diamond particles due to the effect of a thermally softened bronze matrix.

Hyuntaek Na, Gyuyeol Bae, Kicheol Kang, and **Changhee Lee**, Kinetic Spray Coating Laboratory (NRL), Division of Materials Science & Engineering, Hanyang University, 17 Haengdang-dong, Seongdong-gu, Seoul 133-791, Republic of Korea; **Hyungjun Kim**, Welding Research Center, Research Institute of Industrial Science & Technology, San 32 Hyoja-dong, Nam-gu, Pohang 790-600, Republic of Korea; and **Jay-Jung Kim**, Department of Mechanical Engineering, Hanyang University, 17 Haengdang-dong, Seongdong-gu, Seoul 133-791, Republic of Korea. Contact e-mail: chlee@hanyang.ac.kr.

2. Experiments

Figure 1 shows the schematic of the hybrid spraying system. Bronze powders were deposited using atmospheric plasma spraying (APS) (3MB-II, Sultzer Metco, Switzerland) to obtain a thermally softened matrix.

Simultaneously, diamond powders were deposited using kinetic spraying (KINETIC 3000, CGT, Germany) to embed thermally less-exposed diamond particles into the thermally softened bronze matrix. Owing to the strong in-flight drag force of the kinetic spray jet (Ref 8), diamond particles can penetrate through the overlapped gas flow zone between the kinetic and APS flow fields. The angle of the kinetic spray gun was between 40° and 45°, and the gun axis of the APS was fixed perpendicular to the surface of the substrate. For comparison to hybrid spraying, blended bronze/diamond feedstock (in a ratio of 85% bronze to 15% diamond (weight fraction)) was deposited using kinetic spraying. Figure 2 shows scanning electron microscopy images, focused ion beam (DB-FIB, FEI, Netherlands)/transmission emission microscopy (Tecnai G^2 F30 S-Twin, FEI, Netherlands) (FIB/TEM) images, and size distributions of the initial feedstock. Commercially available nickel-coated diamond (IMD-FN series, ILJIN, Korea) and bronze (CUA02PB, KOJUNDO, Japan) powders were employed. Especially, as shown in Fig. 2(f), the monocrystalline diamond feedstock was employed in these experiments. The size distributions of diamond and bronze feedstock were obtained using a laser-assisted particle size analyzer (Microtrac-X100, Honeywell, USA). The mean size of the diamond feedstock was 106 μm, including the nickel layer. Nickel film (mean thickness of 13 μm) was adopted from the previously

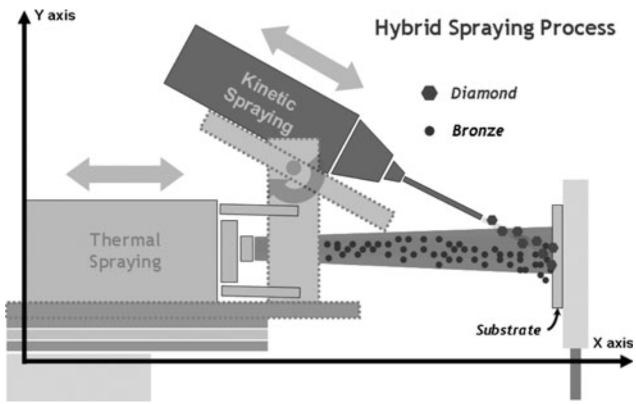

Fig. 1 Schematic of the hybrid spraying process

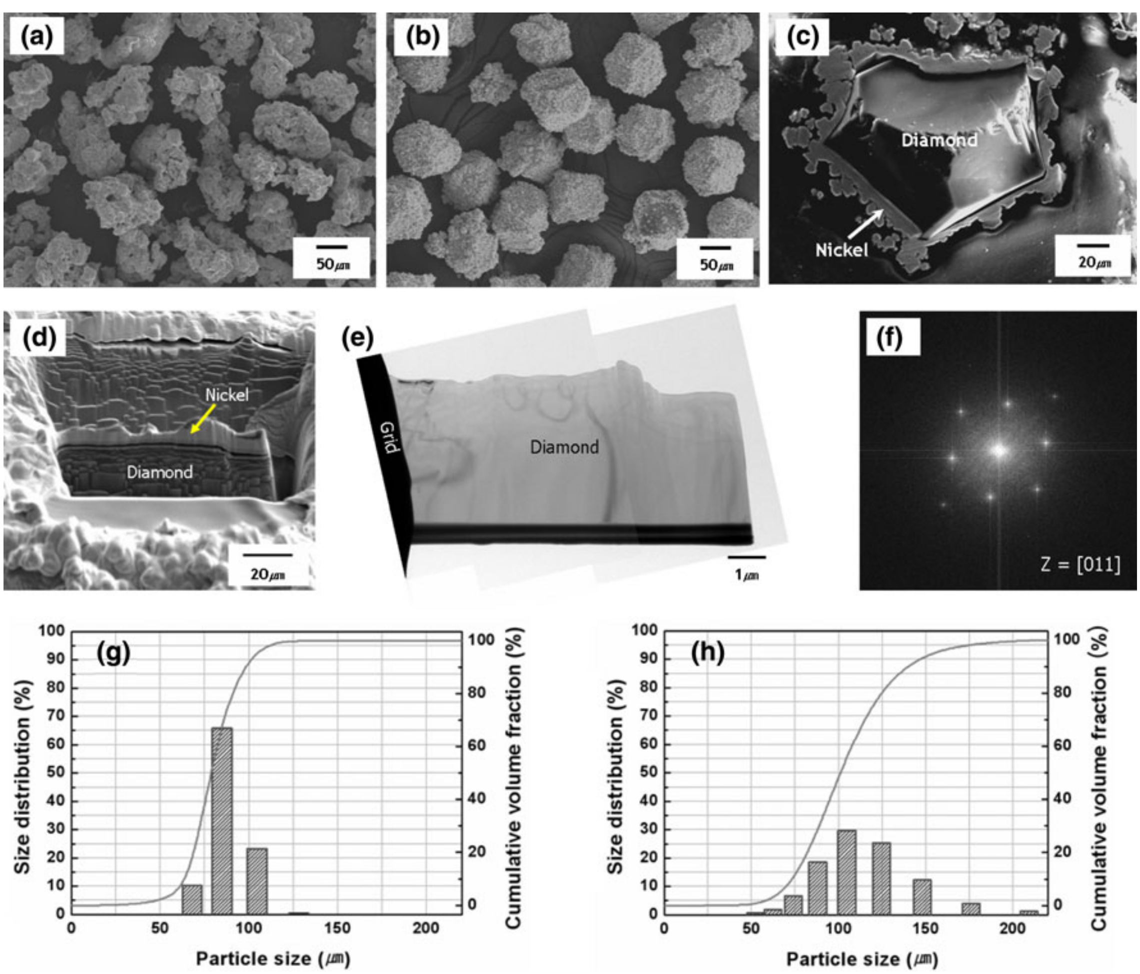

Fig. 2 SEM morphologies of (a) bronze, (b) diamond feedstock, and (c) cross section of a diamond particle. (d and e) FIB/TEM specimen preparation, (f) FFT pattern of a section of a diamond particle, and size distributions of (g) bronze and (h) diamond feedstock

Table 1 Parameters of kinetic spraying

Feedstock	Process gas	Pressure	Temperature	Invariables
Bronze/diamond blended powder (85:15 wt.%)	N_2	2.5 MPa	773 K	Substrate: Al 6061-T6 Gun speed: 50 mm/s Feed rate: 11-15 g/min Spray distance: 50 mm Spray angle to substrate: 90°

Table 2 Parameters of hybrid spraying

Kinetic spraying		APS		Invariables
Feedstock	Diamond	Feedstock	Bronze	Substrate: Al 6061-T6
Process gas	N_2	Current	500 mA	Gun speed: 50 mm/s
Pressure	2.5 MPa	H_2 flow rate	2.35 lpm	
Temperature	773 K	Ar flow rate	47 lpm	
Feed rate	2-5 g/min	Feed rate	12-35 g/min	
Spray distance	30 mm	Spray distance	100 mm	
Spray angle to substrate	45°	Spray angle to substrate	90°	

studied concepts (Ref 5) to achieve successful embedding and uniform flight behavior. Bronze powders were sieved to obtain a mean size of 84 μm using a vibratory sieve shaker (Analysette 3, FRITSCH GmbH, Germany). Roughened aluminum 6061-T6 alloy substrates were prepared using grit blasting, and the substrates were subsequently cleaned by supersonic washing. The detailed process parameters of kinetic and hybrid spraying are given in Table 1 and 2, respectively. Scanning electron microscopy (SEM) (JEOL-5300, JEOL, Japan) and an electron probe micro analyzer (EPMA) (JXA-8100, JEOL, Japan) were used to characterize the coatings. The size of the embedded diamond particles in the composite coatings were estimated using an image analyzer (IMAGE PRO-PLUS 6.0, MEDIA CYBERNETICS, USA). Twenty coating microstructures (1500×2230 μm^2 in dimension) were analyzed and averaged.

3. Computational Simulations

3.1 Model Geometry and the Mesh

The effects of the thermally softened bronze matrix that prevents fracturing of diamond particles during hybrid spraying were simulated and compared to kinetic spraying with finite element analysis (FEA) using ABAQUS/Explicit code (Version 6.7-2) (Ref 9) due to the nature of the high speed, nonlinear transient responses in the solutions. An axisymmetric model was designed as shown in Fig. 3. Three-node linear axisymmetric stress triangle elements (CAX3) without adaptive remeshing were adopted to estimate and investigate equivalent (Von-Mises) flow stress propagations upon impact in the diamond particles.

3.2 Impact Conditions

As shown in Fig. 3, it was assumed that the initial shape of the diamond was spherical, and that the size of the particle and protective layer remained fixed at 80 and 13 μm, respectively. The fully bonded state (between the diamond particle and nickel layer) was assumed using tie-constraints (Ref 9). The deposited matrix layer was assumed to be planar due to the flattening characteristics of the sprayed bronze particles. The temperature of the diamond and nickel protective layer prior to impact was

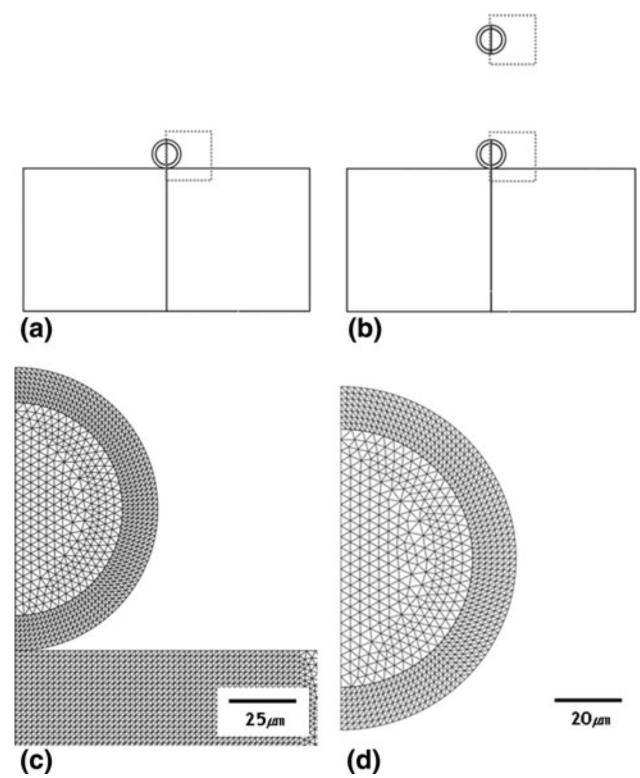

Fig. 3 Initial geometry and mesh of the finite element model for impact simulations: (a) geometry for a diamond/bronze collision, (b) geometry for a diamond/diamond collision, and (c and d) initial state of the mesh

assumed to be room temperature (298 K), while the temperatures of the bronze matrix were assumed to be from 298 to 1040 K for kinetic and hybrid spraying. The bronze particles (consist of 80 wt.% copper and 20 wt.% tin) can be fully solidified below 1073 K. During APS process, almost all the bronze particles were deposited in liquid state due to the extremely high temperature of plasma field (the temperature of the plasma decreases from approximately 12500 to 2500 K with increasing spray distance; Ref 10), and after the deposition, rapid solidification dominantly occurred (Ref 11). In the hybrid spraying process, during formation of bronze matrix layer using APS, diamond particles can be embedded immediately following full solidification of bronze matrix using kinetic spraying based on relatively much faster kinetic gas flow (300-1200 m s^{-1}; Ref 12). Hence, for the simulation, the maximum reasonable temperature of bronze matrix layer (1040 K) was assumed to be just below the peritectic temperature (1073 K). However, in the kinetic spraying, the temperature of the supersonic gas flow sharply decreased through a converge/diverge nozzle (Ref 13). Hence, the temperature of the kinetic sprayed bronze layer was assumed to be room temperature (298 K). Two impact behaviors were considered: diamond/bronze collisions and diamond/diamond collisions. The interaction between the particle and gas flow field (i.e., the velocity reduction due to the bow-shock effect; Ref 14) were not considered for this study. The linear elastic response of diamond (with an elastic modulus of 925 GPa and Poisson's ratio of 0.2) on impact was considered. In order to describe the high-strain-rate plastic deformation of the nickel layer and bronze matrix, the Johnson-Cook plasticity model (Ref 9, 15) was employed. Equivalent (Von-Mises) flow stress propagation, recoverable strain energy, and rebounding velocity in the diamond impact were investigated and analyzed. Other detailed modeling conditions and constitutive equations are provided in the references (Ref 5, 15).

4. Results and Discussion

4.1 Size Distribution of the Diamond Particles in the Composite Coating

Figures 4 and 5 show typical SEM and EPMA images of cross-sectional bronze/diamond composite coatings deposited via kinetic and hybrid spraying. As shown in Fig. 4(a), (b), and 5(a), the diamond particles were uniformly distributed; however, the size of almost all of the embedded diamond particles (1-20 μm) in the matrix material deposited by kinetic spraying only were much smaller than the initial particle size (mean size of 80 μm). In addition, Fig. 5(a) shows that the nickel layer was completely fractured and separated from the diamond particles during impact, and scattered in the coating. Although uniform flight behavior between the diamond and bronze particles was obtained by optimizing the thickness of the nickel film, large diamond particles could not be protected during kinetic spraying. In contrast to the kinetic sprayed results, the cross-sectional SEM image of the composite coating deposited by hybrid spraying shows uniformly distributed diamond particles without a noticeable reduction in size (Fig. 4c, d). In addition, as shown in Fig. 5(b), the diamond particles were fully or partially surrounded by nickel. Figure 6(c) illustrates the

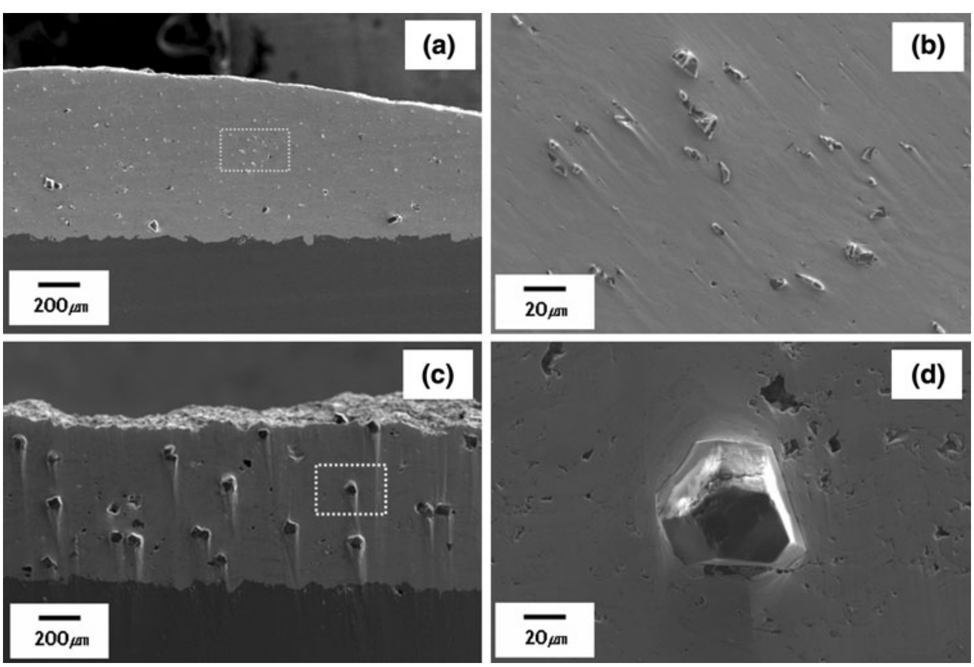

Fig. 4 SEM micrographs of cross-sectional bronze/diamond composite coatings via (a and b) kinetic and (c and d) hybrid spraying

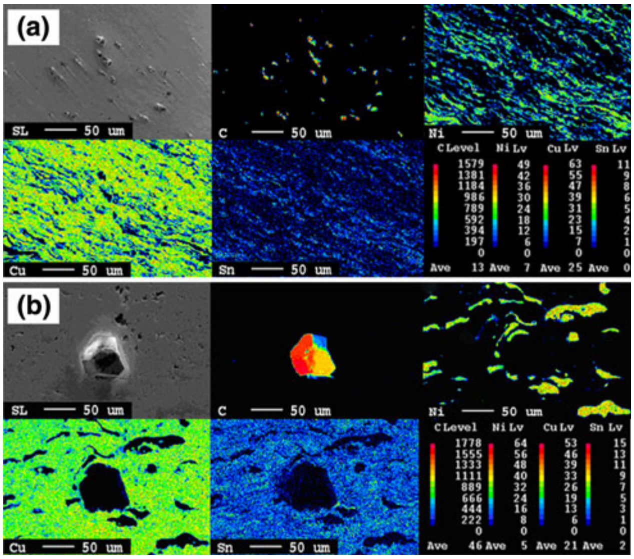

Fig. 5 EPMA chemical mapping images of cross-sectional bronze/diamond composite coatings via (a) kinetic and (b) hybrid spraying (taken from Fig. 4)

diamond size distribution from scanned images of cross-sectional coating layer produced by kinetic and hybrid spraying, as shown in Fig. 6(a) and (b). As shown in Fig. 6(c), the size reduction of the diamond particles embedded by kinetic spraying was much higher than those embedded by hybrid spraying. The mean size of the kinetic sprayed diamond particles was estimated to be 10 μm from Fig. 6(a) and (c). In spite of the protective nickel film, the broken ratio of the diamonds was higher than 87% as calculated by the following theoretical equation (Ref 5).

$$\text{Broken ratio (\%)} = \left(1 - \frac{\text{Mean size of diamond present in the coating}}{\text{Mean size of diamond feedstock } (= 80\,\mu\text{m})}\right) \times 100 \qquad \text{(Eq 1)}$$

In contrast, the mean size of hybrid sprayed diamond particles was estimated as 73 μm from Fig. 6(b) and (c), and the broken ratio of the diamonds was less than 10%.

4.2 Fracture Behavior of Kinetic Sprayed Diamonds with Increasing Size

In general, the kinetic energy of the particles in the kinetic spray gas flow field is based on the competitive relationship between particle size and velocity as described by the basic kinetic energy equation:

$$E_{\text{Kinetic}} = \frac{1}{2}\left(\frac{\pi \cdot d^3 \cdot \rho}{6}\right) v^2 \qquad \text{(Eq 2)}$$

where ρ, *d,* and *v* are the density, diameter, and velocity of the particle, respectively. In Eq 2, the particle size (*d*) is the dominant factor compared to the particle velocity (*v*). In particular, the velocity of an in-flight particle in the

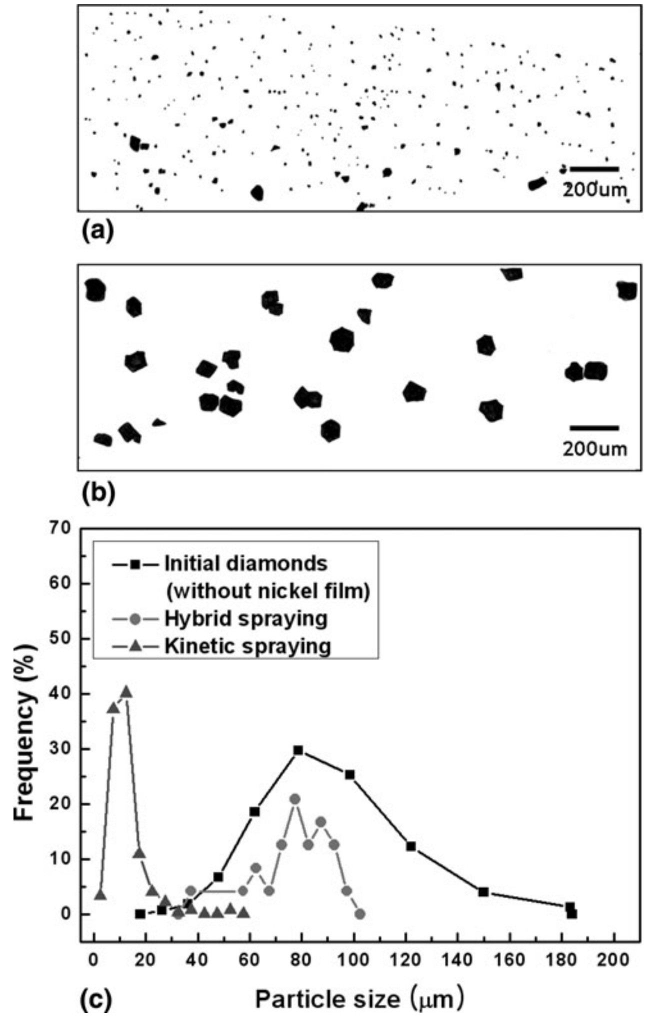

Fig. 6 Image analyses of diamond size distributions in the cross-sectional coatings: scanned images from (a) kinetic and (b) hybrid sprayed composite coating (taken from Fig. 4), and (c) comparison of diamond particles size distributions between the initial state and the coatings

kinetic gas flow decreases with increasing particle size according to Eq 3 (Ref 16):

$$V_{\text{p}} = \frac{1}{\frac{1}{M}\sqrt{\frac{M}{\gamma RT} + 0.85\sqrt{\frac{D}{x}}\sqrt{\frac{\rho_{\text{p}}}{P_0}}}} \qquad \text{(Eq 3)}$$

where V_{p}, M, γ, R, T, D, χ, ρ_{p}, P_0 are particle velocity, molecular weight of the gas, ratio of the specific heat of gas, molar gas constant, gas temperature, particle diameter, position of paraxial ray, particle density, and gas pressure, respectively. However, as shown in Fig. 7, the kinetic energy of the in-flight particle increased due to the size factor, implying that the impact stress was increased with increasing particle size. For instance, in the previously studied 26-μm mean size nickel-coated diamond case, the flight velocity and kinetic energy of the diamond in the kinetic gas flow were 570 m s^{-1} and 9.59×10^{-6} J,

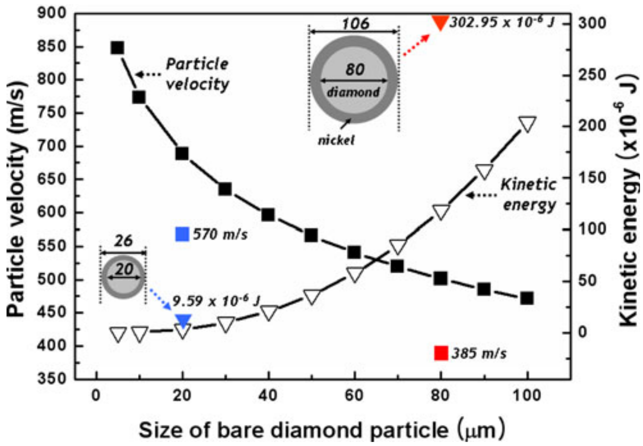

Fig. 7 Flight velocities and kinetic energies of diamond particles with increasing particle size in the kinetic gas flow field

respectively. In contrast, in the 106-μm mean size nickel-coated diamond case, the flight velocity of the diamond (385 m s^{-1}) was lower, but the kinetic energy (302.95×10^{-6} J) was much higher than that of the 26-μm mean size nickel-coated diamond. Figure 8 shows the simulation results of diamond particle embedded onto a bronze matrix during kinetic spraying at an impact velocity of 385 m s^{-1}. Figure 8(a) and (b) shows the simulation results of the nickel-coated diamond at 28 ns in which the maximum impact stress during deposition was observed, and a fully deformed shape was seen at 875 ns, respectively. As shown in Fig. 8(a), the maximum impact stress between the diamond particle and the bronze matrix (6.24 GPa) was slightly higher than the diamond fracture stress (5.8 GPa). However, the impact stress was decreased during deposition as the stress dissipated into the plastic deformation of the nickel layer and bronze matrix, as shown in Fig. 8(b). The estimated impact stress at contact was 3.33 GPa. From these results, it is obvious that the diamond particles with a protective nickel film were not easily fractured during impact with a bronze matrix in this experiment. However, as previously mentioned in Fig. 8(a), diamond fracturing can be initiated due to the high kinetic energy attributed to increased particle size. In addition, as mentioned in the previous studies (Ref 3, 5), it is well known that hard diamond particles can be primarily deposited by embedding, which implies that sufficient kinetic energy of the diamond particles should be obtained to improve deposition efficiency. However, from this study, kinetic spraying showed an adequate range of kinetic energy separating successful embedding and fracturing of diamond particles. Further research is needed to elucidate this complex process more clearly. Figure 8(c) shows the impact stress between the diamond particles in the kinetic gas flow. It was assumed that one diamond particle rebounded after the impact with the bronze matrix. and subsequently another diamond particle collided with the rebounding particle. As a result, the maximum impact stress (25.63 GPa) was much higher

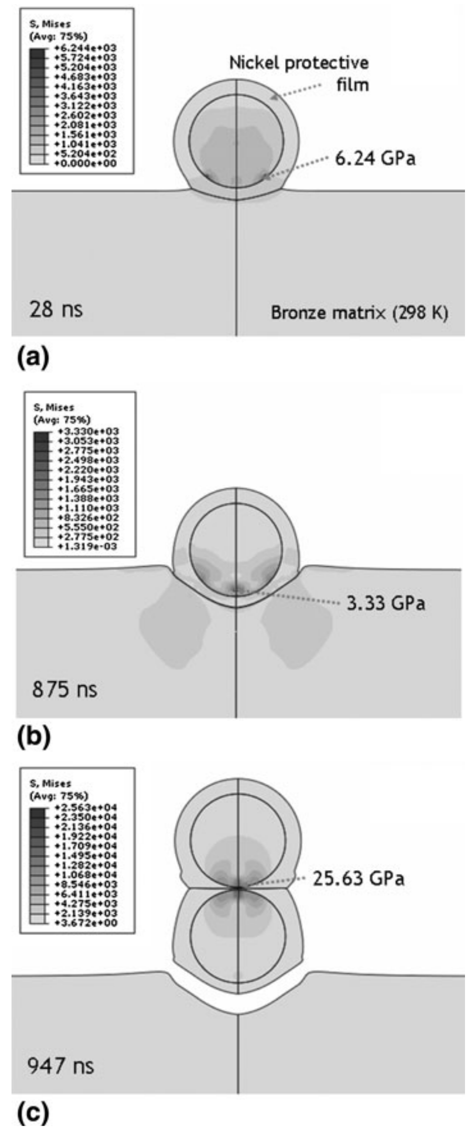

Fig. 8 Finite element analysis of the impact behavior of diamond particles in the kinetic spraying process: images of impact stress profiles of a diamond with the bronze matrix at (a) the maximum value, (b) after complete embedding, and (c) the impact stress propagation between diamond particles

than the diamond fracture stress, leading to severe fracturing of the diamond particles.

4.3 Protection of Diamonds by Thermally Softened Bronze Matrix

Figure 9 shows the simulation results of impact behaviors from hybrid spraying with the same flight velocity as above (385 m s^{-1}). In contrast to the kinetic spraying, Fig. 9(a) shows that the maximum impact stress value (5.27 GPa) was less than the diamond fracture stress. Figure 9(b) shows that the diamond particle was more deeply embedded into the bronze matrix as compared to the kinetic spraying. Still collision between the

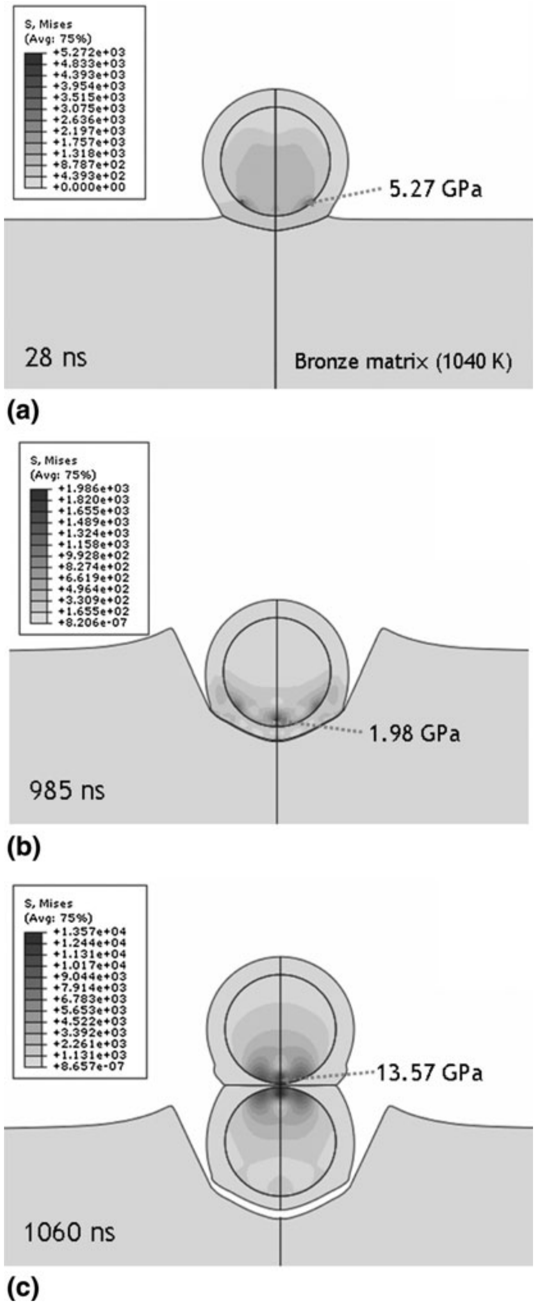

Fig. 9 Finite element analysis of impact behavior of diamond particles in the hybrid spraying process: images of impact stress profiles of a diamond with the bronze matrix at (a) the maximum value, (b) after complete embedding, and (c) the impact stress propagation between diamond particles

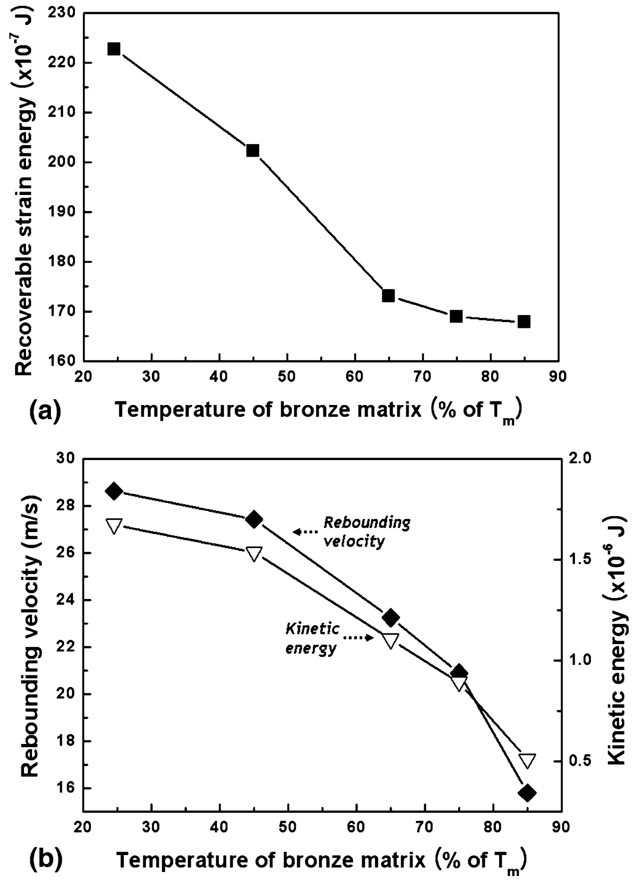

Fig. 10 Effect of the thermally softened bronze matrix layer: (a) recoverable strain energy and (b) rebounding velocity and kinetic energy of the diamond particles as a function of the bronze matrix temperature

rebounded diamond particle and in-flight diamond particle yielded an impact stress value (13.57 GPa) that was higher than the diamond fracture stress (Fig. 9c). However, the maximum impact stress between diamond particles (13.57 GPa) was much less than the previous mentioned kinetic-sprayed results (25.63 GPa). Figure 10(a) shows the recoverable strain energy of the diamond particle after impact with the bronze matrix. From Fig. 10(a), the recoverable strain energy of the diamond particle decreased with increasing temperature of the bronze matrix layer. As previously mentioned, in the hybrid spraying system, bronze particles were deposited by APS in a fully or partially melted state. Hence, thermal softening of bronze can be obtained with the hybrid spraying. After impact of the diamond particle with the bronze matrix, the initial kinetic energy of the diamond particle was primarily dissipated into plastic deformation and the viscous effect/friction works of the impacting particle and matrix according to Eq 4 (Ref 15):

$$\begin{aligned} E_{\mathrm{K}} &= E_{\mathrm{U}} + E_{\mathrm{F}} = (E_{\mathrm{I}} + E_{\mathrm{V}}) + E_{\mathrm{F}} \\ &= \{(E_{\mathrm{P}} + E_{\mathrm{R}}) + E_{\mathrm{V}}\} + E_{\mathrm{F}} \end{aligned} \qquad \text{(Eq 4)}$$

where E_{K}, E_{U}, E_{F}, E_{I}, E_{V}, E_{P}, and E_{R} are the initial kinetic energy of the in-flight particle, internal energy per unit mass, energy dissipated by friction work between the contact surfaces, remaining internal energy, energy dissipated by viscous effects, energy dissipated by plastic deformation, and recoverable strain energy, respectively. However, only a few percent of the initial kinetic energy is normally dissipated by friction work and viscous effects (Ref 15). Therefore, it could be assumed that the initial kinetic energy of an in-flight particle (E_K) was primarily transformed into plastic deformation energy (E_P) and recoverable strain energy (E_R).The initial kinetic energy of the in-flight particle (E_K) can be expressed as follows (Ref 15):

$$E_K = E_I = E_P + E_R = \int_0^t \left(\int_V \sigma^c : \dot{\varepsilon}^{pl} \, dV \right) d\tau + \int_0^t \left(\int_V \sigma^c : \dot{\varepsilon}^{el} \, dV \right) d\tau \qquad \text{(Eq 5)}$$

where σ^c, $\dot{\varepsilon}^{el}$, and $\dot{\varepsilon}^{pl}$ are the stress derived from the constitutive equation (the Johnson-Cook model; Ref 9, 15), the elastic strain rate, and the plastic strain rate, respectively. During the impact between diamond particle and the bronze matrix in hybrid spraying, the matrix experiences more severe plastic deformation due to the thermal softening effect. After impact, the shock wave from the diamond particle completely propagates into the thermally softened bronze matrix causing severe plastic deformation, and a relatively small amount of energy is transformed into recoverable strain energy (E_R). Therefore, as shown in Fig. 10(b), the rebounding velocity of a diamond particle after impact with a bronze matrix decreased due to reduction in recoverable strain energy, and the resultant kinetic energy of the rebounded diamond particle decreased as calculated by the conventional equation (Eq 2). In light of the above discussion, in the hybrid spraying process, almost every diamond particle could be embedded into the bronze matrix layer without rebounding. As a result, the impact stress between diamond particles was significantly less than that in kinetic spraying (Fig. 8 and 9).

5. Conclusion

In this study, composite coatings consisting of a bronze matrix and a relatively large nickel-coated diamond particle (mean size: 106 μm with nickel film) were deposited using a kinetic and an innovative hybrid spraying process. The impact behaviors of feedstock (diamond/bronze and diamond/diamond collision) during each process were simulated with FEA using ABAQUS/Explicit code (Version 6.7-2). Although the thickness of the nickel film was optimized for impact barrier and uniform flight behavior, the diamonds were completely fractured (broken ratio was higher than 87%) during kinetic spraying due to high kinetic energy with increasing particle size. However, size protection of the relatively large diamond particles in bronze/diamond composite coatings was successfully achieved by hybrid spraying (broken ratio was estimated to be less than 10%). It was observed from FEA analysis that impact between hard and brittle diamond particles was one of the main factors affecting the diamond fracture in the coating. Although extremely high kinetic energy was obtained in the larger diamond particles due to the size effect, the diamond particles were efficiently protected during diamond/diamond collisions by reduced recoverable strain energy due to the thermally softened bronze matrix layer in hybrid spraying. In addition, fracture of the diamond particle could be reduced during impact with relatively soft bronze matrix by the protective nickel film in kinetic and hybrid spraying. However, as previously mentioned, fracturing of diamond can be initiated because of high kinetic energy attributed to increased particle size. Therefore, there is an optimum range of kinetic energy separating successful embedding and fracturing of diamond particles in the spraying process. Further research is required to elucidate this complex deposition behavior (such as diamond fraction) more clearly.

Acknowledgments

This research was supported by a grant from the Center for Advanced Materials Processing of the 21st Century Frontier R&D Program (PM003-7-01-01), and the Korean Science Engineering Foundation (2006-02289).

References

1. W. Li, Y. Wang, S. Fan, and J. Xu, Wear of Diamond Grinding Wheels and Material Removal Rate of Silicon Nitrides under Different Machining Conditions, *Mater. Lett.*, 2007, **61**, p 54-58
2. Q.S. Chang, H. Xie, W. Zhang, H. Ye, and P. Hing, Preferential Oxidation of Diamond{111}, *J. Phys. D Appl. Phys.*, 2000, **33**, p 2196-2199
3. S. Shin, Y. Xiong, Y. Ji, H.J. Kim, and C. Lee, The Influence of Process Parameters on Deposition Characteristics of a Soft/Hard Composite Coating in Kinetic Spray Process, *Appl. Surf. Sci.*, 2008, **254**, p 2269-2275
4. T.H. VanSteenkiste, A. Elmoursi, D. Gorkiewicz, and B. Gillispie, Fracture Study of Aluminum Composite Coatings Produced by the Kinetic Spray Method, *Surf. Coat. Technol.*, 2005, **194**, p 103-110
5. H. Na, G. Bae, S. Shin, S. Kumar, H.J. Kim, and C. Lee, Advanced Deposition Characteristics of Kinetic Sprayed Bronze/Diamond Composite by Tailoring Feedstock Properties, *Compos. Sci. Technol.*, 2009, **69**, p 463-468
6. E. Irissou, J.G. Legoux, C. Moreau, and A.N. Ryabinin, How Cold is Cold Spray? An Experimental Study of the Heat Transfer to the Substrate in Cold Gas Dynamic Spraying, *Thermal Spray 2008: Crossing Borders*, E. Lugscheider, Ed., ASM International, Materials Park, OH, 2008
7. H. Assadi, F. Gärtner, T. Stoltenhoff, and H. Kreye, Bonding Mechanism in Cold Gas Spraying, *Acta Mater.*, 2003, **51**, p 4379-4394
8. J. Pattison, S. Celotto, A. Khan, and W. O'Neill, Standoff Distance and Bow Shock Phenomena in the Cold Spray Process, *Surf. Coat. Technol.*, 2008, **202**, p 1443-1454
9. Hibbitt, Karlsson, and Soerensen, ABAQUS™ 6.7-2 User Manual, Pawtucket, RI, USA, 2007
10. B. Liu, T. Zhang, and D.T. Gawne, Computational Analysis of the Influence of Process Parameters on the Flow Field of a Plasma Jet, *Surf. Coat. Technol.*, 2000, **132**, p 202-216
11. S. Sampath and H. Herman, Rapid Solidification and Microstructure Development During Plasma Spray Deposition, *J. Therm. Spray Techol.*, 1996, **5**(4), p 445-456
12. W.Y. Li, H. Liao, C.J. Li, G. Li, C. Coddet, and X. Wang, On High Velocity Impact of Micro-Sized Metallic Particles in Cold Spraying, *Appl. Surf. Sci.*, 2006, **253**, p 2852-2862

13. K. Sakaki and Y. Shimizu, Effect of the Increase in the Entrance Convergent Section Length of the Gun Nozzle on the High-Velocity Oxygen Fuel and Cold Spray Process, *J. Therm. Spray Technol.*, 2001, **10**, p 487-496
14. D.L. Gilmore, R.C. Dykhuizen, R.A. Neiser, T.J. Roemer, and N.F. Smith, Particle Velocity and Deposition Efficiency in the Cold Spray Process, *J. Therm. Sci. Technol.*, 1999, **8**, p 576-582
15. G. Bae, Y. Xiong, S. Kumar, K. Kang, and C. Lee, General Aspects of Interface Bonding in Kinetic Sprayed Coatings, *Acta Mater.*, 2008, **56**, p 4858-4868
16. J. Wu, H. Fang, S.H. Yoon, H.J. Kim, and C. Lee, Measurement of Particle Velocity and Characterization of Deposition in Aluminum Alloy Kinetic Spraying Process, *Appl. Surf. Sci.*, 2005, **252**, p 1368-1377